Journal of Materials Chemistry C

Accepted Manuscript

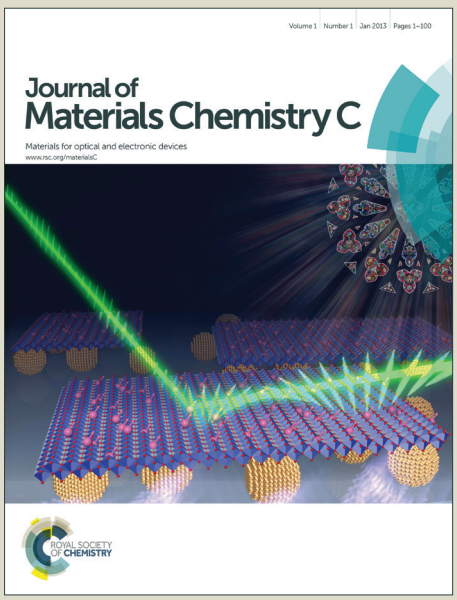

ROYAL SOCIETY OF CHEMISTRY

www.rsc.org/materialsC

Fabrication of high-performance composite electrodes composed of multiwalled carbon nanotubes and glycerol-doped poly(3,4-ethylenedioxythiophene):polystyrene sulfonate for use in organic devices

Dong-Jin Yun[1], Yong Jin Jeong[1], Hyemin Ra[1], Jung-Min Kim[1], Tae Kyu An[1], Minsu Seol[1], Jaeyoung Jang[2], Chan Eon Park[1], Shi-Woo Rhee[1] and Dae Sung Chung[3,*]

[1]Department of Chemical Engineering, Pohang University of Science and Technology (POSTECH), Pohang 790-784, Korea

[2]Department of Energy Engineering, Hanyang University, Seoul 133-791, Korea

[3]School of Chemical Engineering and Material Science, Chung-Ang University, Seoul 156-756, Korea

*Electronic mail: dchung@cau.ac.kr

2nd revision submitted to *Journal of Materials Chemistry C*
Jun 03, 2015

ABSTRACT

In this study, composite films composed of highly conductive multiwalled carbon nanotubes (MWCNTs) and poly(3,4-ethylenedioxythiophene) polymerized with poly(4-styrenesulfonate) (PEDOT:PSS) were fabricated via additional organic-compound doping. The effects of glycerol (GL) or dimethyl sulfoxide (DMSO) doping on the film properties, such as surface roughness, work function (Φ), and conductivity, were studied for both PEDOT:PSS and MWCNT/PEDOT:PSS composite systems. The interactive couplings between the PEDOT and PSS molecules became disordered upon doping with GL or DMSO, which altered the conjugated structure between the PEDOT and PSS chains. Therefore, the electrical conductivity of the PEDOT:PSS and MWCNT/PEDOT:PSS films were enhanced by the addition of GL or DMSO molecules. The GL-doped PEDOT:PSS (PEGL) and ultraviolet (UV)-oxidized MWCNT/PEDOT:PSS (0.2-UVGL) films exhibited comparable work functions (PEGL = 4.87 eV, 0.2-UVGL = 5.0 eV). They also had lower sheet resistances (R_s; PEGL = 806.7 ± 50 Ω/□, 0.2-UVGL = 613 ± 120 Ω/□) as compared to those of the undoped PEDOT:PSS (Φ = 4.92 eV, R_s = 1.03 ± 0.10 MΩ/□) and MWCNT/PEDOT:PSS composites (Φ = 4.7 eV, R_s = 2184 ± 244 Ω/□). Furthermore, because of these excellent electrical properties, the doped MWCNT/PEDOT:PSS films showed great potential as the source/drain electrode in an organic thin-film transistor and as the catalytic counter electrode in a dye-sensitized solar cell. In conclusion, devices with 0.2-UVGL electrodes performed better than the corresponding devices with other MWCNT/PEDOT:PSS composite electrodes and the device characteristics were comparable to that of standard devices with platinum/fluorine-doped tin oxide electrodes

Keywords: Multiwalled carbon nanotube, poly(3,4-ethylenedioxythiophene) polymerized with poly(4-styrenesulfonate), glycerol, organic thin film transistor, dye-sensitized solar cell

1. INTRODUCTION

Many research groups have studied organic-based electrode materials for organic electronics, such as organic thin-film transistors (OTFTs), organic photovoltaic (OPV) devices, dye-sensitized solar cells (DSSCs), and organic light-emitting diodes (OLEDs), with the aim of improving the performance of these devices using low-cost materials and processes.[1-4] Carbon nanotubes (CNTs) are an attractive candidate for electrode materials in various next-generation electronic devices because of their high conductivity, stability, flexibility, and optical transmittance.[3,5-8] CNT-based materials have been applied to various devices, including OLEDs, OTFTs, OPV devices, and DSSCs, as emitting, catalytic, or transparent electrodes.[9-12] However, their poor dispersibility in common solvents is a serious issue that has yet to be fully resolved, despite the continued efforts of numerous research groups.[13,14] Currently, the oxidation of CNTs and grafting of polymers onto CNTs are the most widely utilized methods to enhance their dispersion in solvents.[13-18] In contrast to the CNT oxidation process, the grafting of polymers onto CNTs can enhance the solubility of CNTs in polar solvents without degrading the inherent electrical and physical properties of the CNTs. Furthermore, by combining various polymers, the surface and bulk properties of the CNT composite films can be tailored to specific situations.[17-20] Among the various polymers used, poly(3,4-ethylenedioxythiophene) polymerized with poly(4-styrenesulfonate) (PEDOT: PSS) has outstanding properties for use as a CNT surfactant. By uniformly wrapping CNT chains with PEDOT:PSS, the electrical properties of the CNTs, such as electrical conductivity ($0.1–10^5$ S/cm) and work function (Φ), can be enhanced; moreover, the dispersion of the CNTs in polar and organic solvents can be improved.[17-23] Because of these advantages, many studies on the applications of CNT/PEDOT:PSS composite films have been performed.[17,18,24-26] Recently, our group carried out research on novel preparation

processes for highly functional multiwalled carbon nanotube (MWCNT)/PEDOT:PSS composite electrodes.[24-26] In accordance with our fabrication methods, the MWCNT/PEDOT:PSS composite film can be simply prepared with low-temperature (<150 °C) solution-based processes and still act as a high-performance electrode material with a high work function, surface area, and conductivity. By optimizing the concentration of MWCNTs and subjecting them to ultraviolet (UV) oxidation, the film properties of the MWCNT/PEDOT:PSS composite can be adjusted to meet the requirements of the device.[25] Nevertheless, depending on the oxidation process of the MWCNT/PEDOT:PSS composite system, the trade-off between the work function and conductivity is still an issue for many applications.[24,25]

On the other hand, a PEDOT:PSS film exhibits vastly different electrical conductivities depending on the molecular arrangements between the conducting PEDOT and insulating PSS. Therefore, to easily make conformational changes to a PEDOT:PSS film, the doping of the PEDOT:PSS solution with organic compounds has been used for decades.[27-31] While doping can have many different effects on a system, we believe that doping the MWCNT/PEDOT:PSS solution with a suitable compound can further enhance the film conductivity without sacrificing its work function.

To date, the effects of organic-compound doping on the properties of MWCNT/PEDOT:PSS composite films have not been studied. Therefore, to enhance their electrical performance further when used as electrodes in organic devices, various organic-compound doping processes were applied to MWCNT/PEDOT:PSS composite systems. The MWCNT/PEDOT:PSS composite films were spin-coated onto a 300-nm-thick, thermally grown, SiO_2 layer on Si substrates, and the properties of such films were characterized, including their resistivity, work function, chemical structure, and morphology. By employing the doped MWCNT/PEDOT:PSS films as electrodes, pentacene-based OTFTs,

complementary inverters, and DSSCs were fabricated and their performance was investigated.

2. EXPERIMENTAL SECTION

Figure 1 outlines the preparation processes for the MWCNT/PEDOT:PSS solutions and electrodes, which were used as catalytic counter electrodes in DSSCs and source/drain (S/D) electrodes in OTFTs.

2.1. Composite Solution and Electrode Preparation

The PEDOT:PSS solution (CLEVIOS^{TM} PH500, 1 wt.% in water) and MWCNTs were purchased from H.C. Starck and Carbon Nano-Material Technology Co., respectively. Both the as-purchased MWCNTs and PEDOT:PSS-wrapped MWCNTs were examined with high-resolution transmission electron microscopy (TEM, JEM-2200FS, JOEL) to observe the shape, length, and number of walls. To prepare the oxidized MWCNTs (OMWCNTs), the as-purchased MWCNTs were refluxed in a sulfuric:nitric acid mixture (volume ratio = 3:1) at 100 °C for 1 h, filtered with a polycarbonate membrane (pore size = 0.2 μm), and dried in a vacuum oven at 60 °C for 24 h. The UV-ozone-treated MWCNTs (UVMWCNTs) were prepared with a UV light (wavelength ≈ 254 nm)-ozone treatment using a high-intensity mercury lamp in a UV-tip cleaner (UV/Ozone Procleaner^{TM}, BIOFORCE) for 6 h. Compared to the as-purchased MWCNTs, the loading concentration of OMWCNTs in the PEDOT:PSS solution can be higher because of the functionalization of the carbon backbone and edges of the OMWCNTs.[23,28] The organic dopants used were glycerol (GL) and dimethyl sulfoxide (DMSO), and the optimized doping concentration was found to be 5 vol.% of the PEDOT:PSS solution. After adding the optimized concentrations of MWCNTs and dopants into the PEDOT:PSS solution, it was immediately mixed with an ultrasonicator for 30 min at

room temperature. After the mixing process, the MWCNTs and dopants were well dispersed throughout the PEDOT:PSS solution, except when the solution was overloaded with them, and remained stable without any sedimentation for more than a week.

To fabricate the electrodes, MWCNT/PEDOT:PSS films were prepared on 300-nm-thick SiO_2/N++Si (Silicon Materials Inc.) substrates with solution-based processes (spin or spray coating) at room temperature and atmospheric pressure. The films were then annealed in a vacuum oven at 100 °C for 2 h.

2.2. Device Fabrication

Pentacene-based TFTs with MWCNT/PEDOT:PSS S/D electrodes were fabricated and their performance was characterized. An octadecyltrichlorosilane (OTS) monolayer was formed on the oxide surface to reduce the surface energy and carrier-trap sites at the pentacene/gate dielectric interface. Prior to the formation of the OTS monolayer, the 300-nm-thick SiO_2/N++Si substrate was dipped in piranha solution (H_2SO_4:H_2O_2 = 7:4 vol.%) for 1 h at 100 °C and cleaned in the UV-tip cleaner for 30 min. The clean substrate was then dipped in the 1 mM OTS-toluene solution (purchased from Aldrich Chemical Co.) for 2 h at 4 °C and consecutively washed with toluene and acetone for 30 min per solvent in an ultrasonic bath. Finally, the OTS-treated substrate was annealed in a vacuum chamber for 2 h at 150 °C and then kept in the vacuum chamber at 50 °C until it was required.

A lift-off process was used to pattern the S/D electrodes of the pentacene-based OTFTs. A photoresist (negative-type PR, AZ5214-E) was spin-coated onto the substrate at a speed of 5000 rpm for 45 s, exposed to UV light (major wavelength = 350 nm) through the mask, and then washed out with developer and deionized water. The substrate was subsequently exposed to UV-ozone in the UV-tip cleaner for 10 min, and the MWCNT/PEDOT:PSS film

for the S/D electrode was spin-coated (5000 rpm) onto the entire substrate surface. The substrate was then annealed in a vacuum oven at 100 °C for 2 h and washed with acetone in the ultrasonic bath. Details of the patterning process used on the MWCNT/PEDOT:PSS film to create the S/D electrodes of the OTFTs can be found in the literature.[22,23] Pentacene films, the organic semiconductor in the OTFTs, were deposited with an organic molecular beam deposition (OMBD) system at a pressure of 2×10^{-6} Torr, a temperature of 70 °C, and a deposition rate of approximately 0.2–0.3 Å/s. This fabrication procedure was also utilized to prepare the p-type part of an inverter (channel length = 100 μm, channel width = 1000 μm), and n-type organic semiconductor (*N,N'*-ditridecyl perylene diimide [PTCDI-C13]) films were deposited at room temperature with a rate of approximately 0.2–0.3 Å/s using the OMBD system.

To study the effects of doping on the performance of the MWCNT/PEDOT:PSS composite films when used as catalytic counter electrodes (CCEs), DSSCs with MWCNT/PEDOT:PSS CCEs were also fabricated. The transparent TiO_2 nanoparticle layers were prepared from TiO_2 nanoparticle pastes (Ti-Nanoxide HT/SP from Solaronix) that were screen-printed onto fluorine-doped, tin-oxide-coated (FTO, 8 Ω/□) glass substrates. After drying at 120 °C, the electrode was annealed at 500 °C for 30 min in air. The working electrodes were soaked in a 50 mM solution of $TiCl_4$ for 30 min at 70 °C, and after rinsing with water, the annealing process at 500 °C was performed again for 30 min. For the dye, the working electrodes were immersed in a N719 dye solution (0.3 mM in a 1:1 mixture of acetonitrile and tert-butanol) for 1 day. The substrates were then rinsed with ethanol and dried with a stream of nitrogen gas. The MWCNT/PEDOT:PSS CCEs were prepared on both FTO-coated (8 Ω/□, thickness ≈ 700 nm) and FTO-free glass with spin and spray coating processes, respectively. A Pt/FTO counter electrode system was used as a reference to compare with the catalytic activities of

the MWCNT/PEDOT:PSS CCEs. After preparing the working and counter electrodes, the hot-melt ionomer film was sandwiched between the TiO_2 working electrode and counter electrode by heating the system to 120 °C for a few seconds. The space between the electrodes was filled with a liquid electrolyte consisting of 0.6 M of 1-butyl-3-methyl imidazolium iodide, 0.03 M of I_2, 0.1 M of guanidinium thiocyanate, and 0.5 M of 4-tert-butylpyridine in a mixture of acetonitrile and valeronitrile (ratio of vol.% = 85:15).

2.3. Film and Device Characterization

The sheet resistance of the MWCNT/PEDOT:PSS films was measured with the 4-point probe method (Keithley 2400 source meter). The morphology of the MWCNT/PEDOT:PSS films was investigated with optical microscopy (OM), atomic force microscopy (AFM, Veeco Nanoscope V in NCNT), and scanning electron microscopy (SEM, JEOL JSM-7401F). The chemical states and work function of the MWCNT/PEDOT:PSS films were investigated with X-ray and UV photoemission spectroscopy (XPS and UPS, respectively). The secondary cut-off region (E_{cutoff}) and Fermi energy (E_F) were clearly defined and the work function of the MWCNT/PEDOT:PSS films were calculated with Equation (1):[1,24]

$$\Phi = hv\ (21.2\ eV) - E_{cutoff} + E_{Fermi} \quad (1)$$

where hv (21.2 eV) is the incoming photon energy from the He I source. In addition, a −5 V bias was applied to make the boundary in the E_{cutoff} region clear. The current-voltage (I-V) characteristics of the pentacene-based TFTs and inverters were measured at room temperature with an Agilent E5270A precision semiconductor parameter analyzer and a Keithley 4200 semiconductor characterization system. The I-V characteristics of the DSSCs were measured with a solar simulator equipped with a Xenon lamp (300 W). The power of the simulated light was calibrated to AM 1.5 and 100 mW/cm^2 using a standard Si solar cell. The I-V curves were obtained by applying an external bias to the cell and measuring the generated

photocurrent with a source meter (Keithley 2400). The charge-transfer resistances related to the CCE and electrolyte were measured with electrochemical impedance spectroscopy (EIS, from 100 mHz to 100 kHz).

3. RESULTS AND DISCUSSION

The upper left TEM images in Figure 2 show the composite configurations that have formed between the MWCNTs and PEDOT:PSS in solution, as well as the structure of the as-purchased MWCNTs. The as-purchased MWCNTs have between 5 and 15 walls, with the diameter of the MWCNTs varying from 5 to 20 nm, respectively. Irregularly shaped impurities, which are attributed to carbon-based by-products formed during the MWCNT growth process, can be seen on the exterior walls.[17,18,32] On other hand, as shown in Figure 2, two different MWCNT/PEDOT:PSS composites were extracted from the solutions, which consist of the 0.2 g of the as-purchased MWCNTs in the 20 ml of PEDOT:PSS (0.2-MW) and the 0.2 g of the UV-oxidized MWCNTs in the 20 ml of GL-doped PEDOT:PSS (0.2-UVGL). The wrapping structure of the PEDOT:PSS around the MWCNTs was also investigated. All the arrows in Figure 2 indicate the PEDOT:PSS molecules surrounding the MWCNTs, and as can be seen, most of the as-purchased MWCNTs and UVMWCNTs are enclosed in PEDOT:PSS and GL-doped PEDOT:PSS, respectively. However, both types of sample are enclosed in PEDOT:PSS layers with irregular thicknesses and randomly oriented matrices. On the other hand, despite the UV oxidation process, the UVMWCNTs have retained the original backbone structure of the MWCNTs, and on average, the surrounding PEDOT:PSS layers are thicker than that of the as-purchased MWCNTs, as shown in Figure 2. We believe that the increased thickness of the glycerol-doped PEDOT:PSS layer upon UVMWCNT walls can be attributed to the higher viscosity of MWCNT/PEDOT:PSS solution. The glycerol

addition in the MWCNT/PEDOT:PSS solution results in huge growth in viscosity. For example, solutions consisting of 0.2g as-purchased MWCNTs in 20ml of PEDOT:PSS, turn from a liquid to a viscous gel after mixing in a small dose of glycerol (< 5vol% in solution). On the other hand, due to the enhanced dispersion of partially oxidized MWCNTs, 0.2g of UV-oxidized MWCNTs in 20ml of GL-doped PEDOT:PSS forms a completely dispersed suspension without sedimentation.

The effects of GL and DMSO doping on the film properties of PEDOT:PSS were thoroughly investigated. Figure 3(a) shows the variation in the chemical states of the undoped, GL-doped, and DMSO-doped, spin-coated, PEDOT:PSS films. As can be seen, the GL and DMSO doping has changed the molecular composition of PEDOT and PSS in similar ways. In the C 1s spectra, the main asymmetric peak at 284.8 eV is assigned to sp^3 (C-C) and sp^2 carbon-carbon (C=C) bonding, while the tail peaks at 286.2 eV and 287.4 eV are assigned to carbon-sulfur (C-S) and carbon-oxygen (C-O) bonding, respectively. There is also a very small peak at 291.1 eV, indicating the presence of π-π^* transitions in the PEDOT:PSS films.[24] Compared to the undoped PEDOT:PSS film, both the DMSO- and GL-doped PEDOT:PSS films (PEDM and PEGL, respectively) have slightly higher area ratios for the C-O and C-S peaks to the main asymmetric carbon peak, and this result reveals that the distortion of the PEDOT and PSS interactive coupling by organic dopants increases the PEDOT ratio to PSS.[30,31,33] In aqueous PEDOT:PSS solution, through strong ionic interactions between positively charged PEDOT and negatively charged PSS molecules, the hydrophilic PSS chains enable to consistently maintain stable dispersion of hydrophobic PEDOT chains in water.[33-35] Thereby, the molecular distribution between conductive PEDOT and insulating PSS becomes a critical factor effecting on the physical/electrical characteristics of PEDOT:PSS films.[30,31,33,34] The DMSO and GL molecules of high dielectric constant create screening effect in PEDOT-PSS couplings and this effects lead to conformational change

between PEDOT and PSS chains.[30,31,34] Through this transition mechanism, the DMSO and GL doping result in significant effects on the properties of PEDOT:PSS films.

In addition to the C 1s spectra, the chemical states in the O 1s, S 2p, and Na 1s spectra exhibit similar changes in the PEDM and PEGL films. As shown in Figure 3(a), the intensity of the peaks corresponding to the PEDOT chains increases in the O 1s and S 2p spectra, while the intensity of the peaks assigned to $PSS^{-}Na^{+}$ decrease slightly in the Na 1s spectra. Therefore, compared to the undoped PEDOT:PSS film, the relative molecular ratio of PSS to PEDOT in the DMSO- or GL-doped films has decreased.[30,31,34] In consequence of the conformational change between positively charged PEDOT (+) and negative charged PSS (-), both DMSO and GL-doped films has slightly higher PEDOT concentration at surface region than undoped film.[22,34-36] As a result, as well as sheet resistance, the work function of the doped PEDOT:PSS films also decrease.[22,36] Figures 3(b) and (c) show the UPS spectra and sheet resistance, respectively, of the undoped and doped PEDOT:PSS films. The undoped PEDOT:PSS film has a work function of 4.92 eV and sheet resistance of 1.03 ± 0.10 MΩ/□. The DMSO and GL doping has caused little change to the work function (from 4.92 to approximately 4.87 eV), but it has greatly reduced the sheet resistance by 3 orders of magnitude (DMSO-doped = 1256 ± 100 Ω/□, GL-doped = 806.7 ± 50 Ω/□). As shown in Figure 3(d), despite these changes in the electrical and chemical properties of the doped films, the smooth surface (root mean square roughness (R_{rms}) < 0.4 nm) of the PEDOT:PSS films is maintained, with only the size and number of aggregates slightly increasing with DMSO or GL doping.

As a result of the improved conductivity of the doped PEDOT:PSS films, GL doping, which produced a PEDOT:PSS film with a higher conductivity than the DMSO-doped film, was applied to the MWCNT/PEDOT:PSS composite system, and the effects of GL doping on the properties of the film were investigated. The morphology and cross-section of the 0.2-

UVGL film were observed with AFM, SEM, and OM, with the results shown in Figure 4(a). While agglomerated regions are rare, the majority of the composite materials are uniformly distributed throughout the 0.2-UVGL film and compactly interconnected with each other. Therefore, both the morphological and electrical properties of the 0.2-UVGL film are not dominated by the intrinsic material properties of the UVMWCNTs or PEDOT:PSS. Figures 4(b) and (c) show the properties of the 0.2-UVGL film, as well as the properties of the 0.2-UV and 0.2-MW films for comparison purposes. The R_{rms} of the 0.2-UVGL film (28.1 nm, calculated from 5 × 5 mm AFM images) is not much different from that of the 0.2-MW (25.4 nm) and 0.2-UV (29.0 nm) films. However, the 0.2-UVGL film has a much lower sheet resistance (613 ± 120 Ω/□) compared to that of the other films (0.2-MW = 2184 ± 244 Ω/□, 0.2-UV = 1.50×10^4 ± 1400 Ω/□). We believe that the GL doping increases the conductivity of the PEDOT:PSS film, and thus, decreases the sheet resistance of the 0.2-UVGL film. On the other hand, as shown in the secondary cut-offs of the UPS spectra in Figure 4(c), the work function of the 0.2-UVGL film (5.0 eV) is similar to that of the 0.2-UV film (5.1 eV) but higher than that of the 0.2-MW film (4.7 eV).

To investigate the effects of GL doping on the electrode performance, OTFTs and DSSCs with PEDOT:PSS, 0.2-MW, 0.2-UV, and 0.2-UVGL electrodes were fabricated, and the electrical properties of the devices were compared. The field-effect mobility in the saturated regime (V_D = –40 V) was calculated with Equation (2):[1,24,25]

$$I_{DS} = [(WC_i)/(2L)] \times (V_G - V_{th})^2 \times \mu \quad (2)$$

where I_{DS} is the drain current at a specific gate voltage (V_G), W is the channel width, L is the channel length, V_{th} is the threshold voltage, μ is the carrier's field-effect mobility, and C_i is the capacitance per unit area of the gate dielectric (the value of C_i for the 300-nm-thick SiO_2 was determined to be 10 nF/cm^2). Figure 5(a) shows the comparative transfer characteristics

of the pentacene-based TFTs with various MWCNT/PEDOT:PSS composite S/D electrodes, and from the transfer curves, the electrical properties of the electrodes were calculated, with the results summarized in Table 1. As shown by the lower gradient of the PEDOT:PSS plot of $(I_{DS})^{1/2}$ vs. V_G compared to that of the other samples (Figure 5(a)), the PEDOT:PSS S/D electrode could not endure a high current flow at an applied bias greater than - 10 V. The damage caused to this electrode resulted in a low μ value (0.0855 $cm^2/(V \cdot s)$) and a poor on/off ratio (approximately 3×10^5) for the PEDOT:PSS device. On the other hand, because of the high electrical/thermal conductivity and stability, no electrical/physical damage, such as electrode degradation or a current drop at a high bias, occurred while operating the pentacene-based TFTs with MWCNT/PEDOT:PSS composite S/D electrodes (i.e., the 0.2-MW, 0.2-UV, and 0.2-UVGL electrodes). Consequently, the electrical performance of the devices with composite electrodes are better than that of pentacene-based TFT with the PEDOT:PSS S/D electrode. As shown in the transfer/output characteristics (Figures 5(a) and (b)), the pentacene-based TFTs with the 0.2-UV and 0.2-UVGL S/D electrodes have comparable electrical performances, and their values for μ (approximately 0.31 $cm^2/(V \cdot s)$) and on/off ratios (2×10^6) are almost twice that of the pentacene-based TFT with the 0.2-MW S/D electrode. In addition, because of the high electrical performance of the pentacene-based TFT with the 0.2-UVGL electrode, the complementary inverter was fabricated with a 0.2-UVGL S/D electrode, and its electrical properties were characterized. As shown in Figure 5(c), the fabricated complementary inverter shows a good relationship between the output voltage (V_{out}) and input voltage (V_{in}). The V_{out} is maintained at a value that is almost the same as the voltage swing (V_{dd}) at low V_{in} values, and then V_{out} abruptly drops to 0 V at the corresponding V_{in}. This behavior originates from the complementary inverter turning on and off the p- (pentacene) and n-type (PTCDI-C13) TFTs. As shown in Figure 5(d), the DC gain (dV_{out}/dV_{in}) is nearly 60 when V_{dd} is over 50 V.

To account for the differences in electrical performance between the 0.2-MW, 0.2-UV, and 0.2-UVGL S/D electrodes, the hole-injection barrier at the S/D-electrode/pentacene interface was investigated with stepwise deposition and UPS analysis. Generally, the hole-injection barrier, which is a crucial factor for charge-carrier injection at the S/D-electrode/pentacene interface, has an energy gap that is between the work function of the S/D electrode and highest occupied molecular orbital (HOMO) of pentacene.[1,24,25,37] Figures 6(a–c) show the UPS spectra of the HOMO levels of the pentacene/electrode interfaces for the 0.2-UV, 0.2-UVGL, and 0.2-MW electrodes, respectively. From the valence band structure of the pentacene layer (approximately 6.4 nm) grown on the electrodes, the resulting hole-injection barrier for each interface was obtained, as shown in Figure 6(d). The relatively low work function of the 0.2-MW electrode leads to the formation of a higher hole-injection barrier (0.49 eV) to the pentacene layer compared to the other electrodes (0.2-UV = 0.38 eV, 0.2-UVGL = 0.40 eV). Therefore, this higher hole-injection barrier for the 0.2-MW S/D electrode must be one of the reasons for the relatively poor electrical performance of the pentacene-based TFT compared to that of the 0.2-UV and 0.2-UVGL S/D electrodes.

Moreover, because of their excellent conductivity and surface area, the MWCNT/PEDOT:PSS composite films were employed as a CCE instead of the commonly used Pt or Pt/FTO cathodes in DSSCs, and their electrical properties were characterized. The electrode performance was evaluated in accordance with the device characteristics. Figure 7(a) shows the structure of the DSSCs and the equivalent electrical circuit used to study their electrical properties. The DSSCs had identical structures and components except for the CCE electrode used, and thus, the direct influence of CCE material on the performance of the device could be analyzed. The I-V characteristics and cell performance parameters (short-circuit current density (J_{sc}), open circuit voltage (V_{oc}), fill factor (F.F.), and efficiency (η)) of the DSSCs were measured, with the results summarized in Figure 7(b) and Table 2,

respectively. The DSSC with the PEDOT:PSS CCE has the lowest cell performance (J_{sc} = 6.7 mA·cm^{-2}, F.F. = 32.9%, and η = 1.8%) of the CCE materials tested because of its low electrical conductivity and surface area. On the other hand, compared to the PEDOT:PSS CCE, the relatively high conductivity of the PEGL CCE greatly improved J_{sc} from 6.7 to 12.9 mA·cm^{-2}. However, the PEGL CCE has a smaller F.F. because of its low surface area, which is an obstacle to creating a DSSC with high cell efficiency (3.2% in the case of the PEGL CCE). As shown in Table 2, the DSSCs with MWCNT/PEDOT:PSS composite CCEs have higher photoelectronic performances than that with PEGL or PEDOT:PSS CCEs, despite the similar conductivities of the CCE electrodes. In addition to the large surface area of the MWCNTs, their high catalytic activity and electrical conductivity greatly improve the charge transport properties of the MWCNT/PEDOT:PSS CCEs in the DSSCs.[26,38,39] All of the DSSCs with MWCNT/PEDOT:PSS CCEs that were characterized by our group exhibit higher photoelectronic performances than that with the PEDOT:PSS CCE, but there are small differences between the cell efficiencies that are dependent on the electrical conductivities of MWCNT/PEDOT:PSS CCEs. This is why the DSSC with the 0.2-UVGL CCE shows a higher cell efficiency (5.9%) than that of the other MWCNT/PEDOT:PSS CCEs (0.2-MW = 5.6%, 0.2-UV = 5.3%).

On the other hand, the GL doping of the PEDOT:PSS or MWCNT/PEDOT:PSS solutions improves the film conductivity without sacrificing the other film properties, including the catalytic activity and surface area. In addition to the excellent surface area and catalytic activity of the 0.2-UVGL CCE, its electrical conductivity is comparable to that of conducting oxides, e.g., FTO, and therefore, based on its strong performance as both a CCE and conducting electrode, FTO-free DSSCs with PEGL and 0.2-UVGL counter electrodes were fabricated with the spray coating method. A spray gun connected to a source of N_2 gas (99.9 %) was used to spray the PEGL and 0.2-UVGL solutions onto glass substrates at 150

°C, and the film thickness was maintained at approximately 10 μm.[26,39] Despite the absence of the FTO electrode, the DSSCs with spray-coated PEGL and 0.2-UVGL counter electrodes have comparable photoelectronic characteristics to that of the corresponding DSSCs with spin-coated PEGL and 0.2-UVGL CCEs on FTO electrodes. Furthermore, both the spray-coated PEGL and 0.2-UVGL counter electrodes have higher F.F. values than the corresponding spin-coated CCEs on FTO electrodes, as shown in Table 2. Figures 7(c) and (d) show the I-V characteristics and EIS spectra, respectively, of the DSSCs with spray-coated MWCNT/PEDOT:PSS (0.2-UVGL and PEGL) and Pt/FTO counter electrodes. The lower J_{sc} of the DSSC with the spray-coated 0.2-UVGL counter electrode (J_{sc} = 10.4 mA·cm^{-2}, η = 5.6%) results in a lower cell efficiency compared to that with the Pt/FTO counter electrode (J_{sc} = 12.5 mA·cm^{-2}, η = 6.8%). The EIS spectra in Figure 7(d) show why there is a difference between the J_{sc} and η values of the DSSCs with the spray-coated 0.2-UVGL and Pt/FTO counter electrodes. According to the equivalent electrical circuit, the series resistance (R_s, starting point of the first semicircle) of the spray-coated 0.2-UVGL electrode is higher than that of the Pt/FTO electrode. Therefore, because of the large difference in the electron supply capacities between the counter electrode and electrolyte/CCE interface, the DSSC with the spray-coated 0.2-UVGL counter electrode has smaller J_{sc} and η values than that with the Pt/FTO counter electrode. Nevertheless, the lower charge-transfer resistance (R_{ct}, horizontal diameter of the first semicircle) of the spray-coated 0.2-UVGL electrode, which is caused by its excellent catalytic activity, means its F.F. value (64.5 %) is comparable to that of the Pt/FTO electrode (67.8 %).

4. CONCLUSION

We have studied the effects of organic-compound doping on the surface and bulk properties of PEDOT:PSS and MWCNT/PEDOT:PSS composite films. It was found that the organic dopants (GL and DMSO) of high dielectric constant influence the conformational change between PEDOT and PSS chains in the MWCNT/PEDOT:PSS composite films. This in turn greatly increases the electrical conductivity of the films without large changes to other film properties. Consequently, by optimizing the dopant concentration in the MWCNT/PEDOT:PSS solution, well-designed MWCNT/PEDOT:PSS composite films that could be used as high-performance electrodes in OTFTs and DSSCs were prepared. In addition, OTFTs and DSSCs with various MWCNT/PEDOT:PSS composite electrodes were characterized in detail. We found that the GL doped 0.2-UV composite (0.2-UVGL) had a work function comparable to that of the undoped 0.2-UV composite, and it had a higher electrical conductivity than the other composite films tested. Therefore, the 0.2-UVGL film exhibited excellent performance when used as a counter electrode in a DSSC, as well as when employed as an S/D electrode in a pentacene-based TFT.

ACKNOWLEDGMENT

Table 1 Electrical properties of the pentacene TFTs with MWCNT/PEDOT:PSS composite S/D electrodes

S/D electrodes	Field-effect mobility (μ, cm^2/Vs)	On/off current ratio	Threshold voltage (V_{th}, V)	Subthreshold swing (SS, V)
PEDOT:PSS	0.086	3×10^5	0.89	1.20
0.2 MW	0.189	1×10^6	- 2.80	1.28
0.2 UV	0.307	2×10^6	- 1.60	1.22
0.2 UVGL	0.308	2×10^6	- 1.90	1.23

Table 2 Photo electronic characteristics of DSSCs with MWCNT/PEDOT:PSS counter electrodes

Device type	Counter electrode	Electrode coating process	V_{oc}/mV	Jsc/mA cm^{-2}	F. F.	η (%)
Conventional DSSC	PEDOT:PSS/FTO	Spin-coating	829	6.7	32.9	1.8
	PEGL/FTO	Spin-coating	826	12.0	32.5	3.2
	0.2 MW/FTO	Spin-coating	808	12.4	55.7	5.6
	0.2 UV	Spin-coating	808	12.1	54.7	5.3
	0.2 UVGL	Spin-coating	811	12.2	59.6	5.9
	Pt/FTO reference	Drop-casting	826	11.6	66.2	6.3
FTO-free DSSC	PEGL (~ 10 um)	Spray-coating	820	11.3	44.1	4.1
	0.2 UVGL (~ 10 um)	Spray-coating	835	10.4	64.5	5.6

5. References

1. S. Rhee and D. J. Yun, *J. Mater. Chem*., 2010, **18**, 5437.

2. H. Ma, H. L. Yip, F. Huang and A. K. Y. Jen, *Adv. Func. Mater.*, 2010, **20**, 1371.

3. T. N. Murakami and M. Gratzel, *Inorg. Chim. Acta.*, 2008, **361**, 572.

4. K. X. Steirer, J. J. Berry, M. O. Reese, M. F. V. Hest, A. Miedaner, M. W. Liberatore, R. Collins and D. S. Ginley, *Thin Solid Films*, 2009, **517**, 2781.

5. H. Z. Geng, K. K. Kim, K. P. So, Y. S. Lee, Y. Chang and Y. H. Lee, *J. Am. Chem. Soc.*, 2007, **129**, 7758.

6. H. Tantang, J. Y. Ong, C. L. Loh, X. Dong, P. Chen, Y. Chen, X. Hu, L. P. Tan and L. J. Li, *Carbon*, 2009, **47**, 1867.

7. H. Z. Geng, K. K. Kim, C. Song, N. T. Xuyen, S. M. Kim, K. A. Park, D. S. Lee, K. H. An, Y. S. Lee, Y. Chang, Y. J. Lee, J. Y. Choi, A. Benayad and Y. H. Lee, *J. Mater. Chem.*, 2008, **18**, 1261.

8. R. K. Jackson, A. Munro, K. Nebesny, N. Armstrong and S. Graham, *ACS nano*, 2010, **4**, 1377.

9. R. A. Hatton, N. Blanchard, L. W. Tan, G. Latini, F. Cacialli and S. R. P. Silva, *Org. Electron*, 2009, **10**, 388.

10. E. C. Ou, L. Hu, G. C. R. Raymond, O. K. Soo, J. Pan, Z. Zheng, Y. Park, D. Hecht, G. Irvin, P. Drzaic and G. Grunner, *ACS nano*, 2009, **3**, 2258.

11. W. J. Yu, B. R. Kang, I. H. Lee, Y. S. Min and Y. H. Lee, *Adv. Mater.*, 2009, **21**, 4821.

12. C. H. Chang, C. H. Chein and J. Y. Yang, *Appl. Phys. Lett.*, 2007, **91**, 083502.

13. L. Vaisman, G. Marom and H. D. Wagner, *Adv. Func. Mater.*, 2006, **16**, 357.

14. K. K. Kim, S. M. Yoon, J. Y. Choi, J. Lee, B. K. Kim, J. M. Kim, J. H. Lee, U. Paik, M. H. Park, C. W. Yang, K. H. An, Y. Chung and Y. H. Lee, *Adv. Func. Mater.*, 2007, **17**, 1775.

15. V. Datsyuk, M. Kalyva, K. Papagelis, J. Parthenios, D. Tasis, A. Siokou, I. Kallitsis and C. Galiotis, *Carbon*, 2008, **46**, 833.

16. Y. Y. Huang and E. M. Terentjev, *Polymers*, 2012, **4**, 275.

17. P. C. Ma, N. A. Siddiqui, G. Marom and J. K. Kim, *Composite: Part A*, 2010, **41**, 1345.

18. L. Hu, D. S. Hecht and G. Gruner, *Chem. Rev.*, 2010, **110**, 5790.

19. T. M. Wu, Y. W. Lin and C. S. Liao, *Carbon*, 2005, **43**, 734.

20. Y. Chen, K. S. Kang, K. J. Han, K. H. Yoo and J. Kim, *Synth. Met.*, 2009, **159**, 1701.

21. L. Groenendaal, F. Jonas, D. Feitag, H. Pielartzik and J. R. Reynolds, *Adv. Mater.*, 2000, **12**, 482.

22. J. Hwang, F. Amy and A. Kahn, *Org. Electron.*, 2006, **7**, 387.

23. S. K. M. Jonsson, J. Birgerson, X. Crispin, G. Greczynski, W. Osikowicz, A. W. D. Gon, W. R. Salaneck and M. Fahlman, *Synth. Met.*, 2003, **139**, 1.

24. D. J. Yun, K. Hong, S. H. Kim, W. M. Yun, J. Jang, W. S. Kwon, C. Park and S. W. Rhee, *ACS appl. Mater. Interfaces*, 2011, **3**, 43.

25. D. J. Yun and S. W. Rhee, *ACS Appl. Mater. Interfaces*, 2012, **4**, 982.

26. D. J. Yun, H. Ra and S. W. Rhee, *Renew. Ener.*, 2013, **50**, 692.

27. J. Ouyang, Q, Xu, C. W. Chu, Y. Yang, G. Li and J. Shinar, *Polymer*, 2004, **45**, 8443.

28. A. M. Nardes, R. A. J. Janssen and M. Kemerink, *Adv. Func. Mater.*, 2008, **18**, 865.

29. A. M. Nardes, M. Kemerink, R. A. J. Janssen, J. A. M. Bastiaansen, N. M. M. Kiggen, B. M. W. Langeveld, A. J. J. M. van Breemen and M. M. de Kok, *Adv. Mater.*, 2007, **19**, 1196.

30. H. Yan and H. Okuzaki, *Synth. Met.*, 2009, **159**, 2225.

31. A. A. Farah, S. A. Rutledge, A. Schaarschmidt, R. Lai, J. P. Freedman and A. S. Helmy, *J. Appl. Phys.*, 2012, **112**, 113709.

32. I. D. Rosca, F. W. Motohiro and T. Akasaka, *Carbon*, 2005, **43**, 3124.

33. Y. Xia and J. Ouyang, *ACS Appl. Mater. Interfaces.*, 2010, **2**, 474.

34. P. Wilson, C. Lekakou and J. F. Watts, *Org. Electon.*, 2012, **13**, 409.

35. X. Hu, L. Chen, Y. Zhang, Q. Hu, J. Yang and Y. Chen, *Chem. Mat.*, 2014, **26**, 6293.

36 J. Huang, P. F. Miller, J. S. Wilson, A. J. de Mello, J. C. de Mello and D. D. C. Bradley, *Adv. Func. Mater.*, 2005, **15**, 290.

37. B. Kang, S. Lim, W. H. Lee, S. B. Jo and K. Cho, *Adv. Mater.*, 2013, **25**, 5856.

38. J. M. Kim and S. W. Rhee, *Electrochim. Acta*, 2013, **83**, 264.

39. W. Kwon, J. Kim and S. W. Rhee, *J. Mater. Chem. A*, 2013, **1**, 3202.

FIGURE CAPTIONS

Figure 1. An outline of the preparation processes for the MWCNT/PEDOT:PSS solutions and spin-coated films to be used as the CCEs of DSSCs and S/D electrodes of OTFTs.

Figure 2. TEM images of the MWCNT chains that were extracted from different MWCNT/PEDOT:PSS composite solutions: the as-purchased MWCNTs, 0.2-MW, and 0.2-UVGL.

Figure 3. (a) XPS spectra (C 1s, O 1s, S 2p, and Na 1s), **(b)** UPS spectra (secondary cut-off region), **(c)** sheet resistances, and **(d)** morphologies (OM and AFM images) of the undoped, DMSO-doped, and GL-doped PEDOT:PSS films.

Figure 4. (a) The morphologies/cross-sections (OM, AFM and SEM images) of 0.2-UVGL and the comparative graphs including the relationship information for (b) sheet resistance/surface roughness and (c) work function among different MWCNT/PEDOT:PSS composite films (0.2-MW, 0.2-UV and 0.2-UVGL).

Figure 5. Comparative I-V characteristics of the pentacene-based TFTs ((a) transfer and (b) output curves) and complementary inverters ((c) output voltage (V_{out}) - input voltage (V_{in}) characteristics and (d) DC gains (dV_{out}/dV_{in})) with various MWCNT/PEDOT:PSS electrodes.

Figure 6. UPS spectra showing the HOMO levels of the pentacene/electrode interface for: **(a)** 0.2-UV, **(b)** 0.2-UVGL and **(c)** 0.2-MW electrodes. **(d)** The hole-injection barriers for the corresponding interfaces.

Figure 7. (a) Structure and equivalent electrical circuit of the DSSCs fabricated with

various MWCNT/PEDOT:PSS CCEs. I-V characteristics of: **(b)** spin-coated CCEs on FTO electrodes and **(c)** spray-coated counter electrodes. **(d)** EIS spectra of the DSSCs with Pt on FTO and spray-coated 0.2-UVGL CCEs.

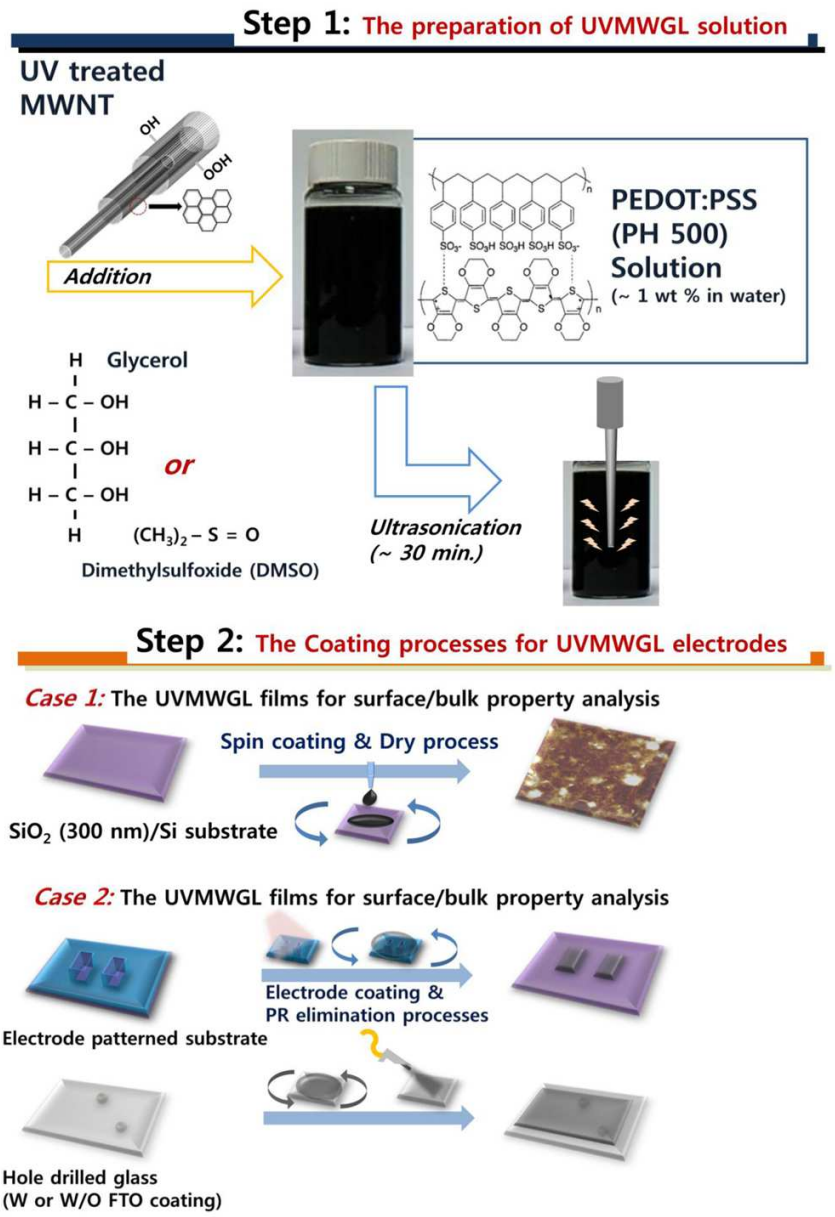

Figure 1. Yun et al.

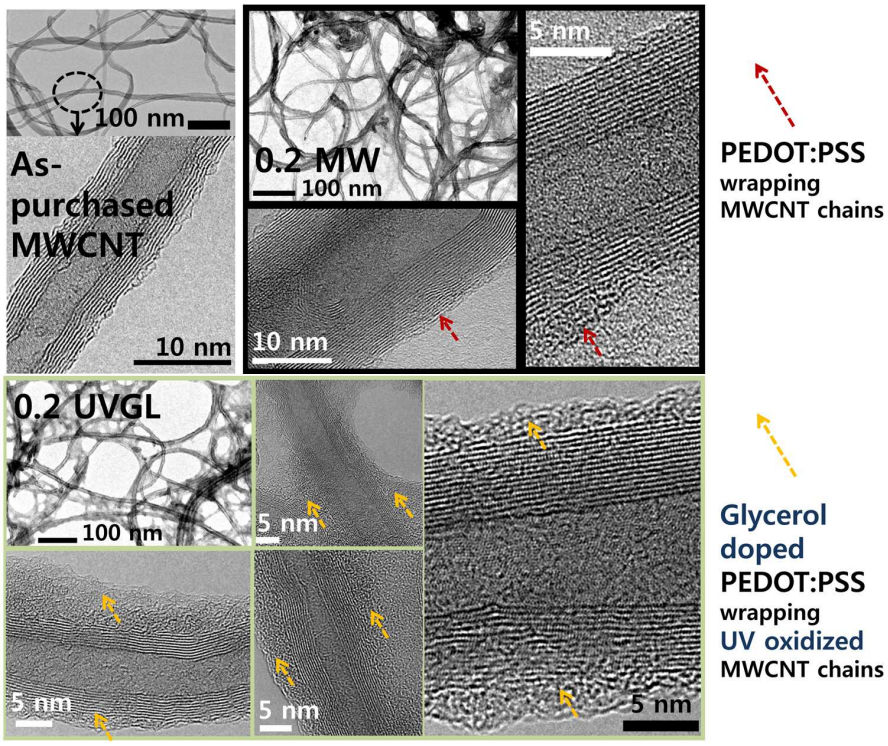

Figure 2. Yun et al.

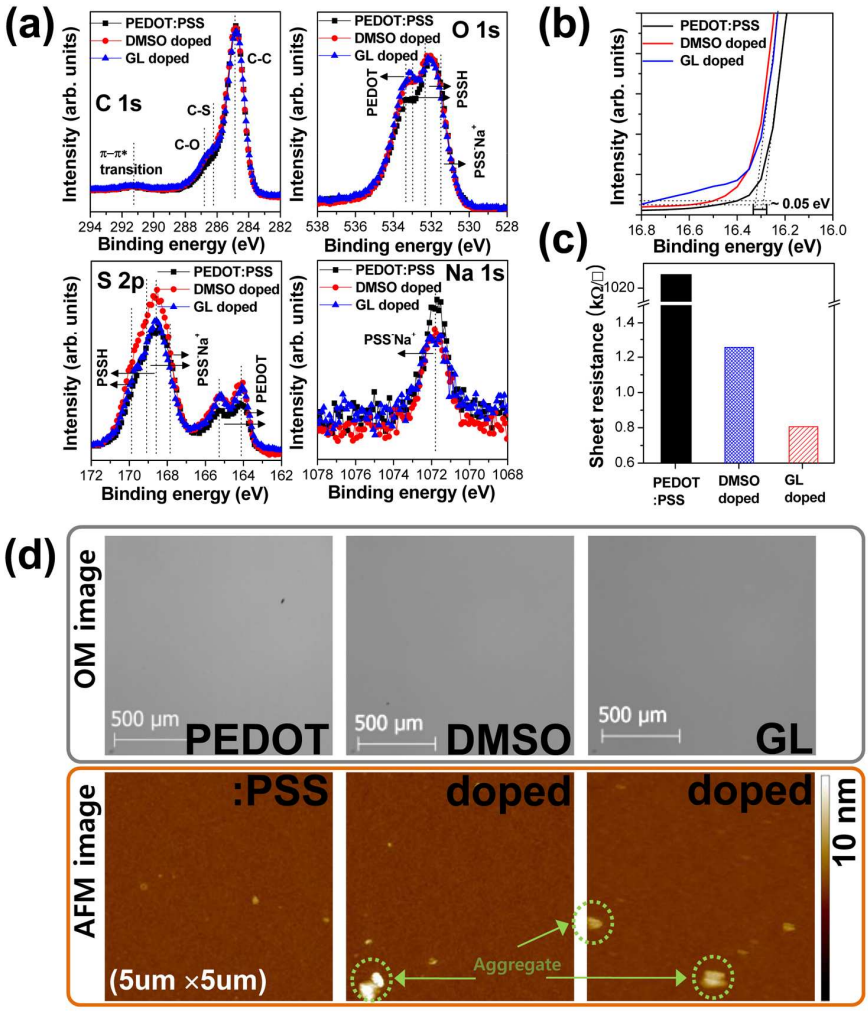

Figure 3. Yun et al.

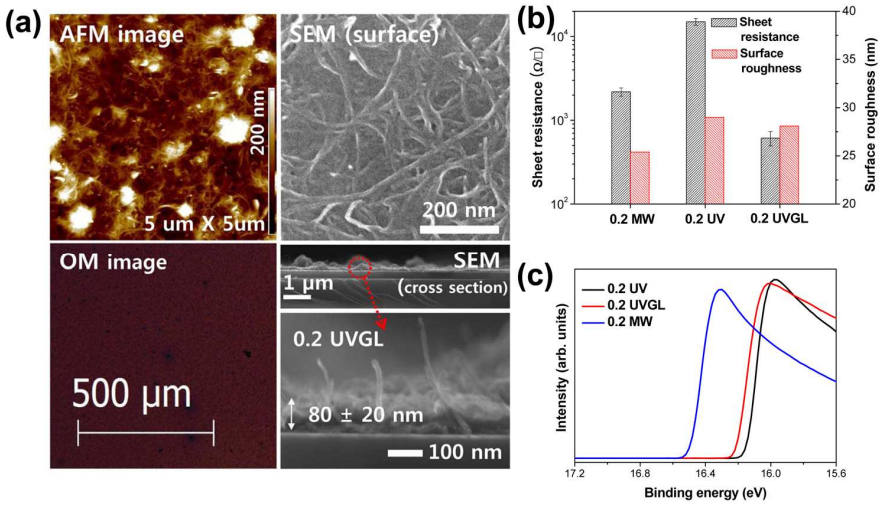

Figure 4. (a) Yun et al.

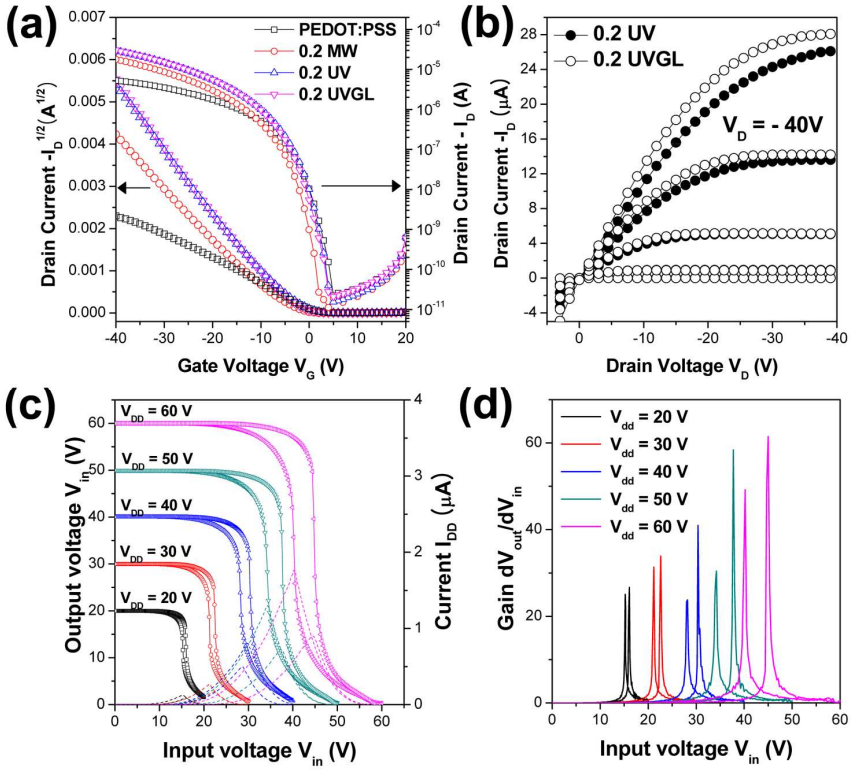

Figure 5. Yun et al.

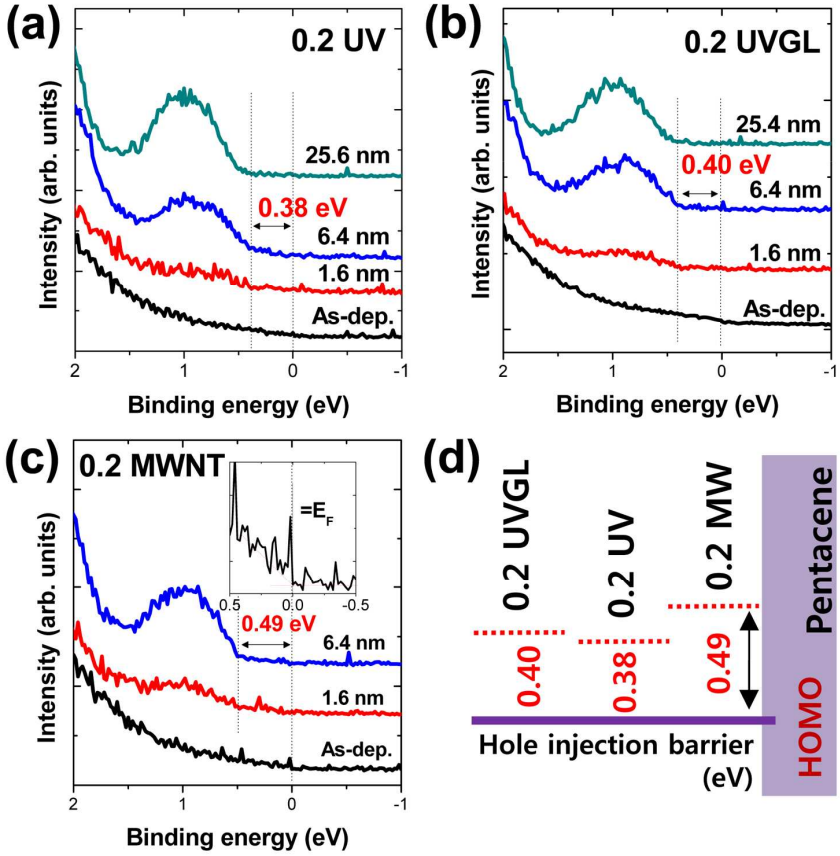

Figure 6. Yun et al.

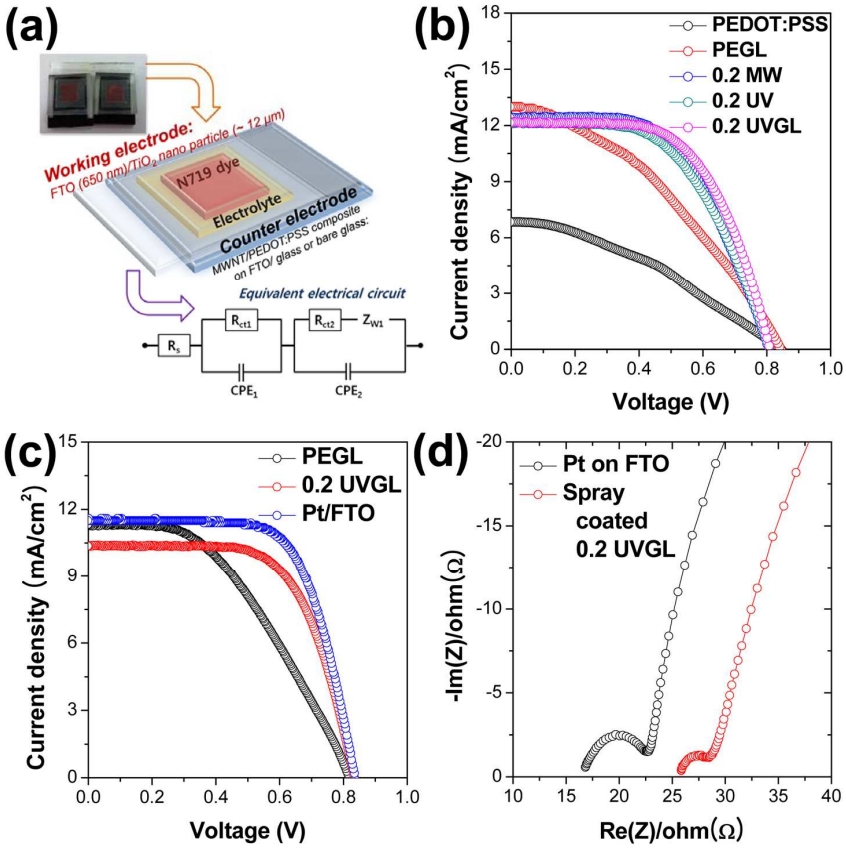

Figure 7. Yun et al.

Table of contents

Figure:

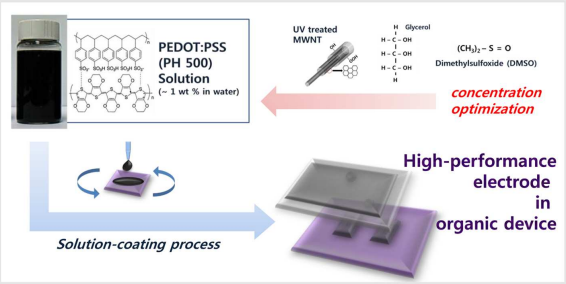

Text:

The optimized organic doping facilitates high performance of MWCNT/PEDOT:PSS composite film as an electrode in organic devices